SSRG International Journal of Electronics and Communication Engineering
ISSN: 2348-8549/ https://doi.org/10.14445/23488549/IJECE-V13I7P114

Volume 13 Issue 7, 203-213, July 2026

Original Article

Shared Aperture Quad-Band Antenna Configuration for 5G Sub-6 GHz and Emerging Mid-Band Scenarios

Manasa K R[1], Pramod Kumar Naik[2], Shashi Kumar D[3]

[1]*Department of ECE, Dayananda Sagar University, Karnataka, India.*
[2]*Department of AI and Robotics, Dayananda Sagar University, Karnataka, India.*
[3]*Department of ECE, Christ University, Karnataka, India.*

[1]*Corresponding Author : manasakr@gmail.com*

Received: 09 May 2026 Revised: 11 June 2026 Accepted: 29 June 2026 Published: 29 July 2026

Abstract - *A novel space-efficient shared-aperture antenna supporting quad-band is proposed for modern wireless and emerging 5G applications. The antenna operates at 2.1 GHz, 2.4 GHz, 3.7 GHz, and 7.8 GHz, targeting key bands such as Band 1/n1, ISM, n77/n78, and n258 extension. Each band is supported by a uniquely scaled octa-star radiating element, formed by overlapping two square patches rotated by 45°, enabling frequency-specific impedance matching and spatial isolation. The novelty of the proposed design lies in the integration of four independently scaled octa-star radiating elements within a shared aperture to achieve compact quad-band operation with high inter-band isolation. An equivalent circuit model abstracts the resonant behavior of each antenna using parallel RLC networks and shared feed components. Simulated and measured results show excellent impedance matching with reflection coefficients of –39.39 dB, –37.94 dB, –29.91dB, and –31.69 dB, and VSWR values close to unity at 2.1 GHz, 2.4 GHz, 3.7 GHz, and 7.8 GHz, respectively. Similarly, the peak gains of 3.62 dBi, 4.22 dBi, 4.34 dBi, and 7.87 dBi are achieved across the respective bands. Inter-band isolation remains below –30 dB, reaching –66.71 dB in some cases. The proposed antenna offers a scalable, fabrication-friendly solution for integration into 5G-enabled devices, IoT gateways, and compact wireless platforms requiring multiband operation within a single aperture.*

Keywords - *Shared-aperture antenna, Quad-band operation, Octa-star patch, 5g Communication, Sustainable electronics.*

1. Introduction

The evolution of wireless communication, especially with the 5G deployment, has increased demand for compact, multiband antennas that can parallelly support diverse services such as LTE, Wi-Fi, IoT, and emerging mid-band applications. Aperture antennas stand out in this context due to their high gain, bandwidth, and low profile, which make them ideal for integration into modern wireless systems.

A shared aperture antenna is a notable advancement in the field of planar antenna designs. This technique allows the integration of multiple applications like radar, communication, and electronic warfare within a single physical structure. This architecture reduces the overall size, weight, cost of fabrication, and complexity in integrating into an application. In addition, this will also mitigate the interference while improving aerodynamic efficiency and reliability, making it particularly advantageous in vehicular, stealth, and mobile applications.

Shared aperture systems utilize frequency, polarization, beam orientation, and timing to manage many signals parallelly. Some designs make use of smart digital techniques to control and steer multiple beams at a time, while others merge different antenna elements into one shared structure, permitting 5G, IoT, and sensing technologies to coexist. As wireless networks keep growing, shared aperture antennas are appropriate in building efficient, compact, and flexible communication systems for the future [1-4].

Nowadays, sub-6 GHz bands have been widely adopted for reliable coverage in 5G networks. Also, mid-band frequencies are gaining importance for balancing coverage and capacity in vehicular communication, industrial IoT, and early 6G applications. Although several dual-band and multiband antenna structures have been reported, they suffer from design complexity or fail to integrate both bands in single aperture.

The proposed work in this paper presents how to address the gap by introducing quad band shared aperture antenna that combines sub-6 GHz and mid-band operation in a compact footprint, ensuring high isolation, which is the need for CubeSat payloads, vehicular V2X systems, and urban base stations. The design pushes multiband antenna technology, minimizes material usage, and electronic waste compared to single-band antennas. The following section covers the latest shared aperture antenna designs used in space, mobile, vehicle, and 5G infrastructure, pointing out their strengths and limitations.

2. Literature Review and Gap Analysis

Recent studies have explored shared-aperture designs across space, smartphones, automobiles, and 5G infrastructure. For CubeSat systems, Uddin et al. [5] proposed a pentaband aperture-in-aperture antenna employing High Impedance Surfaces (HIS) to achieve circular polarization and wideband performance.

Latif et al. [6] integrated S- and X-band communication into a single shared aperture to address space constraints. Elkady et al. [7] combined a spiral and four patch antennas to achieve multiband coverage, through integrating multiple feed ports within the restricted CubeSat dimensions remain challenging.

A shared aperture dual-band dual-polarised antenna is presented by He et al. [8] to achieve reduced coupling and enhance gain. But, the design present limitation of interband coupling as the number of bands increases using this technique. These studies highlight the potential of shared apertures in restricted space environments. But reveal limitations in fabrication complexity and integration feasibility.

From the base station and portable device application point of view, Ji et al. [9] presented a shared aperture method for the integration of multiple frequency bands. It presents an advantage that eliminates the need for extra decoupling, but face difficulty of scalability issues during fabrication. A multilayer PCB enabled dual-band antenna that covers millimetre (mmWave) and sub-6 GHz band suitable for smartphones is demonstrated by Ylä-Oijala et al. [10]. It offers high efficiency and beam steering, yet faces limitations like complexity in the feed network during the extension of frequency bands.

Similarly, Wenguan Cao [11] presents a mmWave and sub-6 GHz frequency band integrated coplanar embedded antenna for base station applications. A dual-band shared aperture magnetoelectric dipole structure with enhanced isolation for a base station is demonstrated by Cao et al. [12]. However, these techniques presenting mmWave and sub-6 GHz bands that integrate excellently, but express limitations like structural complexity due to a large frequency ratio and discrepancy between measurement and simulation. These limitations, in turn, lead to more research in this area.

Shared aperture creations have supported applications like vehicular as well as in MIMO system implementations. Sufian et al. [13] and Zhao et al. [14] make use of metamaterials and layered electromagnetic designs. These structures refine isolation and allow omni- or uni-directional radiation characteristics. Wang et al. [15] proposed a calibration mechanism to a dual-band antenna for phase error correction to increase electromagnetic transparency. Though they express that the system suffers from problems involved with high port density, complex wiring, and grating lobes. However, they acknowledge that the system poses limitations in spatial flexibility and interference between bands that continue to block the successful performance of the shared aperture systems.

The dual-band antenna with calibration mechanism system, is incorporated by Su et al. [16] presented a GPS S-band vehicle-to-vehicle (V2V) shared aperture system that ensures spatial and cost efficiency. These studies collectively highlight the scope of shared aperture research, yet they constantly expressing on persistent need for a solution that balances compactness, feed design simplicity, and reliable multiband functionality.

However, the quad-band shared-aperture antennas featuring compact form factors and simple feed systems have made great strides in recent years; they are still relatively unexplored. In an effort to address this need, a new octa-star-shaped radiating element that operates (in quad-band mode) at four specific frequencies (2.1, 2.4, 3.7, and 7.8 GHz) is presented in the current paper. These four frequency bands correspond to: (a) LTE (2.1 GHz); (b) Wi-Fi/IoT (2.4 GHz); (c) 5G sub-6 GHz (3.7 GHz), and (d) emerging mid-band applications (7.8 GHz). The pattern of the proposed octa-star configuration is made by placing two squares one above the other at an angle of 45° from each other.

By this design, the resonance of each structure can be separated with less interference, and has a much smaller footprint for use in devices like 5G, IoT, and vehicular communication. The novelty lies in combining symmetry-inspired geometry with shared-aperture operation, validated through simulation and measurement, and benchmarked against state-of-the-art designs.

3. Antenna Topology and Analytical Modeling

The proposed structure is depicted in the Figure 1 uses symmetry-based geometry to achieve resonance separation, which prevents interference between different frequency bands. By carefully adjusting the dimensions as shown in Table 1, the design keeps impedance matching requirements to achieve maximum radiation efficiency throughout the four frequency bands. The star shape also keeps things compact and do not require advanced feed systems to work.

For the antenna's physical design and fabrication, FR-4 epoxy substrate with a height of 1.6 mm, dielectric constant (ε_r) of 4.4, and a loss tangent ($\tan\delta$) of 0.02 used. Choosing FR-4 material allows us to achieve mechanical stability, keeping cost low, as the material suits perfectly for standard

PCB production. This specific design offers solid performance for mid-band frequency applications. But it is important to know that FR-4 exhibits a trade-off in reliability, due to its inherent lossy characteristics at higher frequency spectrum.

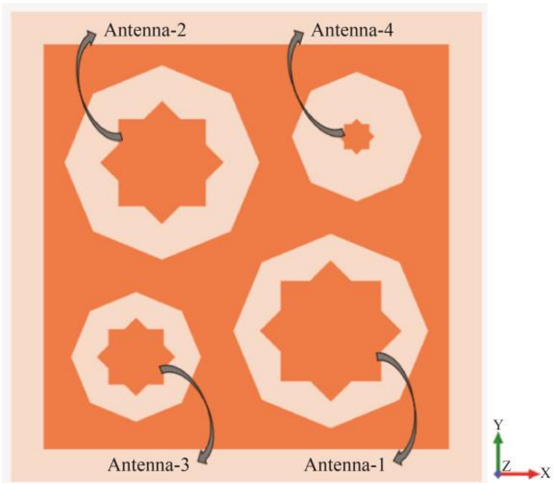

Fig. 1 The proposed structure of shared aperture

Table 1. Slot radius and square sides dimensions of each resonant frequency band

Operating Frequency/Band	Slot Radius (mm)	Square side (mm)
2.1 GHz (Band 1 / n1)	30	30.89
2.4 GHz (ISM band)	30	26.9
3.7 GHz (n77/n78)	20	17.15
7.8 GHz (n258 extension)	20	7.73

The antennas operating at the lower operational bands of 2.1 GHz and 2.4 GHz are placed along the principal diagonal of the square. Similarly, the secondary diagonal houses the antennas functioning at the elevated frequency bands of 3.7 GHz and 7.8 GHz, as depicted in Figures 2 (a) and (b).

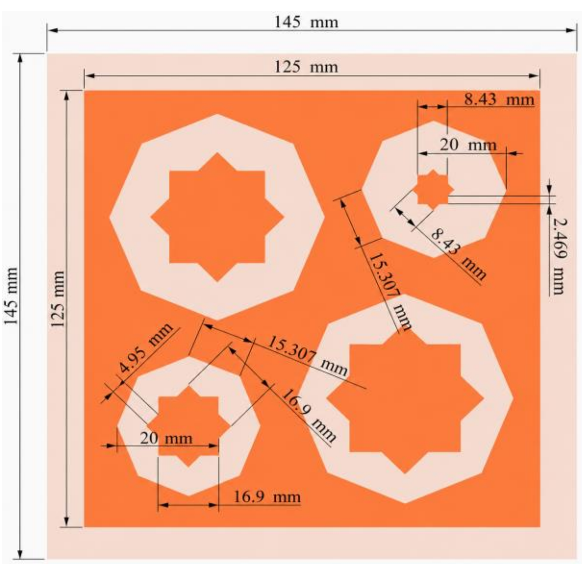

(a)

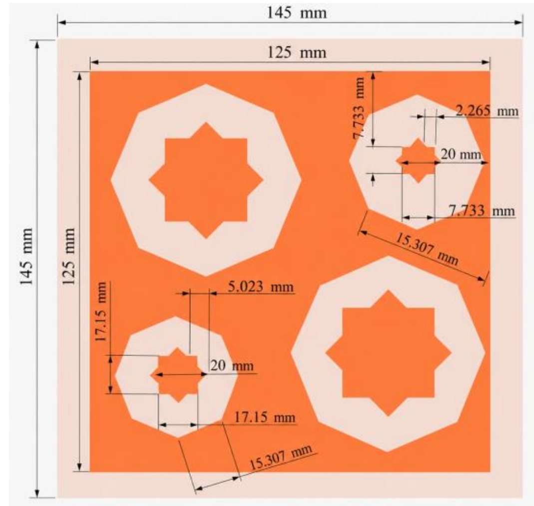

(b)

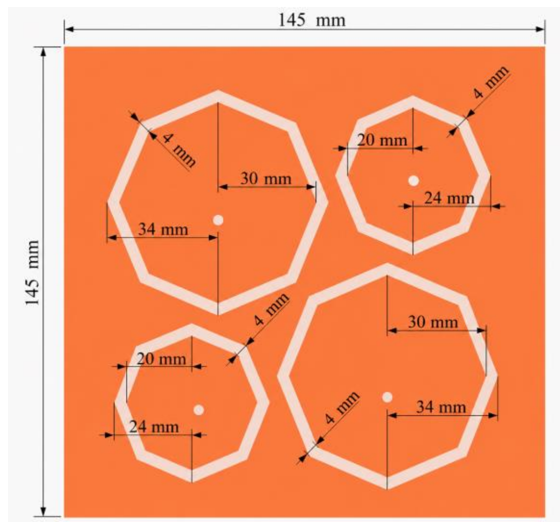

(c)

Fig. 2 Shared-aperture antenna layout (a) & (b) Front view, (c) Rear view.

This logical configuration effectively nullifies undesirable signal interference and ensures the integrity of the signal pattern through the equidistant placement of the radiating elements.

To further enhance the separation, in the ground plane, each radiating element in the top layer is allocated a distinct, dedicated aperture, isolated from the primary ground area. These discrete ground regions are achieved through segmentation of the copper layer beneath each aperture, maintaining a separation gap of $4\,mm$ between adjacent regions as shown in Figure 2 (c). The approach adopted in this design aids in decoupling the signals and mitigation of inter-frequency signal bleed.

The comprehensive design architecture streamlines the processes of enabling the incorporation of four distinct frequency bands via adjustments to the dimensions or positioning of the apertures. The proposed approach optimizes the utilization of the foundational material's area. Hence, the design can be more appropriate for IoT gateways, 5G-enabled devices, and vehicular communication systems.

3.1. Equivalent Circuit Representation

The equivalent circuit presented in Figure 3 shows the response of the four individual antennas present in the shared aperture geometry. Each radiating antenna element operating at 2.1 GHz, 2.4 GHz, 3.7 GHz, and 7.8 GHz is modeled using RLC components, capacitance (C_p), inductance (L_p), and resistance (R_p). The input of each antenna includes a series feed inductance (L_f) and capacitance (C_s), which symbolize the electromagnetic connection between the radiating element and the feed network. The individual impedance and the corresponding S_{11} values of each element in the proposed design can be evaluated using Equations (1) and (2) [17].

$$Z_{in} = R_p + j\omega L_p + \frac{1}{j\omega C_p} \quad (1)$$

$$S_{11} = \frac{Z_{in}-Z_0}{Z_{in}+Z_0} \quad (2)$$

Where $Z_0 = 50\,\Omega$ is the reference impedance. These series RLC components influence the impedance matching with each port and ensure effective power delivery with minimal reflection.

The 2.1 GHz antenna has the RLC values of $R_{p1} = 24\,\Omega$, $L_{p1} = 198\,nH$, and $C_{p1} = 29\,pF$, whereas the 2.4 GHz antenna's values are $R_{p2} = 20\,\Omega$, $L_{p2} = 162\,nH$, and $C_{p2} = 28\,pF$. Similarly, for the 3.7 GHz and 7.8 GHz antennas are $R_{p3} = 45\,\Omega$, $L_{p3} = 402\,nH$, $C_{p3} = 23\,pF$ and $R_{p4} = 20\,\Omega$, $L_{p4} = 750\,pH$, $C_{p4} = 3.72\,pF$ respectively.

The resonant frequency of each radiating patch is approximated by:

$$f_r = \frac{c}{2L\sqrt{\epsilon_{eff}}} \quad (3)$$

where c - speed of light,
L - effective patch length, and
ϵ_{eff} - effective dielectric constant.

This relation demonstrates how dimensional tuning directly influences the operating frequency.

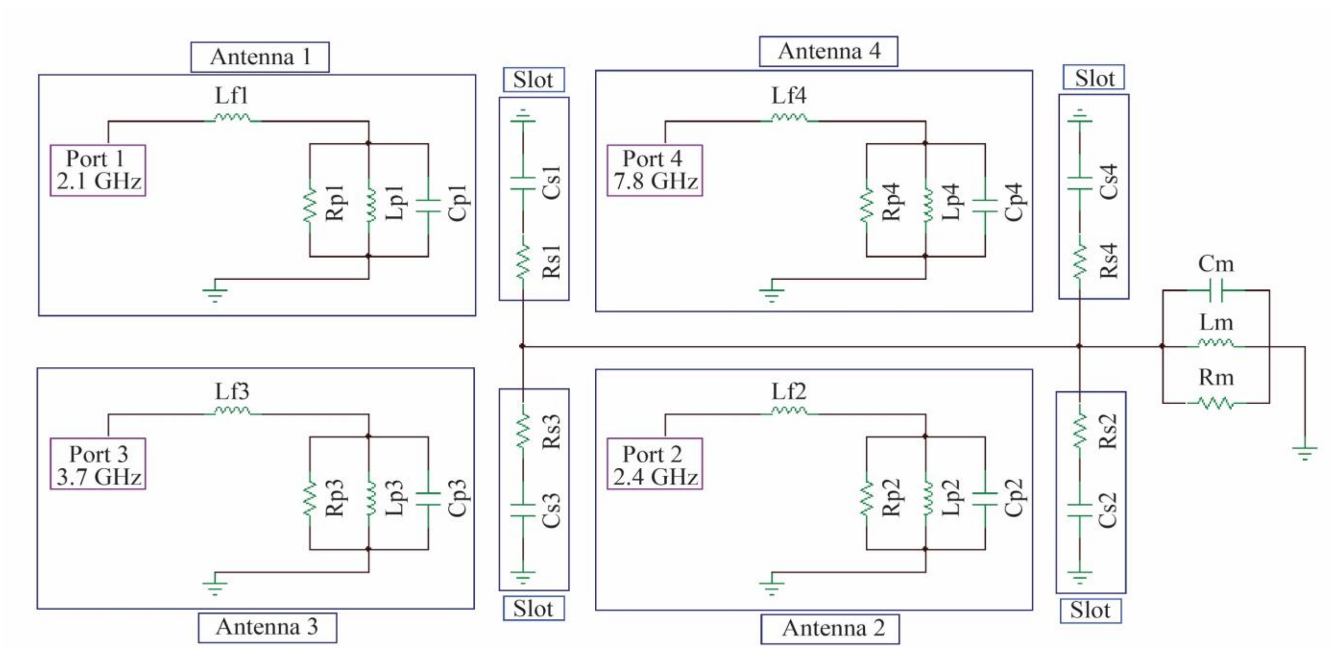

Fig. 3 Equivalent circuit of the introduced shared-aperture

The impacts created by the gaps in the upper layer and bottom layer of the dielectric material are depicted with reactive loads consisting of R_s and C_s elements in series.

The values of these lumped elements change based on the frequency bands. For the 2.1 GHz gap, $R_{s1} = 152.8\,\Omega$ and $C_{s1} = 16.3\,pF$, but for the 7.8 GHz gap, $R_{s4} = 432.6\,\Omega$ and $C_{s4} = 0.99\,pF$.

The approximate capacitance between adjacent ground regions is given by:

$$C_{gap} \approx \frac{\varepsilon_0 \varepsilon_r A}{d} \quad (4)$$

Where A is the overlap area and $d = 4\,mm$ is the separation distance. Increasing d reduces C_{gap}, thereby lowering coupling and enhancing isolation.

Table 2. RLC Parameters for feed, patch, and slot elements across four frequency bands and central patch

Ant 1 2.1 GHz	Ant 2 2.4 GHz	Ant 3 3.7 GHz	Ant 4 7.8 GHz	Main Element
L_{f1} 2.5 nH	L_{f2} 2.2 nH	L_{f3} 1.2 nH	L_{f4} 0.68 nH	R_m 143.32 Ω
R_{p1} 24 Ω	R_{p2} 20 Ω	R_{p3} 45 Ω	R_{p4} 20 Ω	L_m 547.6 pH
L_{p1} 198 nH	L_{p2} 162 nH	L_{p3} 402 pH	L_{p4} 750 pH	C_m 71.55 pF
C_{p1} 29 pF	C_{p2} 28 pF	C_{p3} 23 pF	C_{p4} 3.72 pF	
R_{s1} 152.8 Ω	R_{s2} 186.9 Ω	R_{s3} 234.5 Ω	R_{s4} 432.6 Ω	
C_{s1} 16.3 pF	C_{s2} 1.55 pF	C_{s3} 1.35 pF	C_{s4} 0.99 pF	

To simplify, the primary patch structure is kept identical across all configurations, as shown by $R_m = 143.32\ \Omega$, $L_m = 547.67\ pH$, and $C_m = 71.55\ pF$, which defines the fundamental resonator operating with each gap-fed design. Table 2 provides the RLC component values associated with all four antennas, along with the main patch created in the overall design. This circuit model enables quick study and design optimization without demanding full-wave simulation. It also shows how effectively the fractured ground designs keep electrical impulses apart and how radiating components are distributed.

4. Simulation and Practical Evaluation

To authenticate the effectiveness of the developed shared-aperture antenna system, both full-wave electromagnetic simulations and experimental measurements were conducted across all four frequency bands. This section presents a comparative analysis of key parameters such as gain distribution, Voltage Standing Wave Ratio (VSWR), Isolation, and reflection coefficient (S_{11}), both H-plane and E-plane Co-polarization and Cross-polarization characteristics.

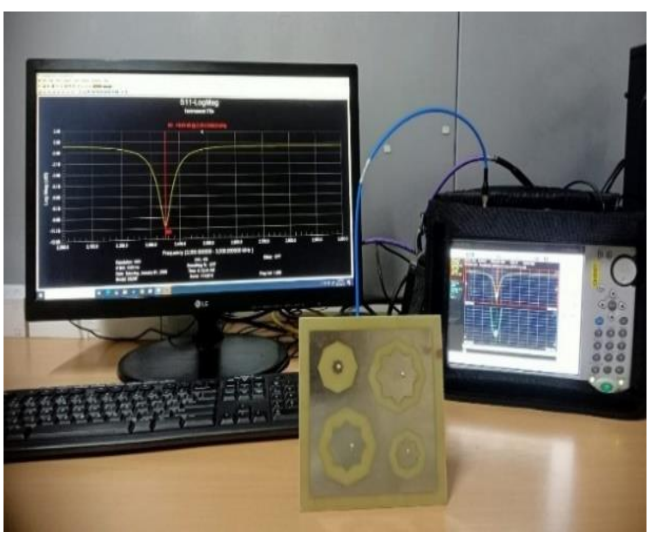

(a)

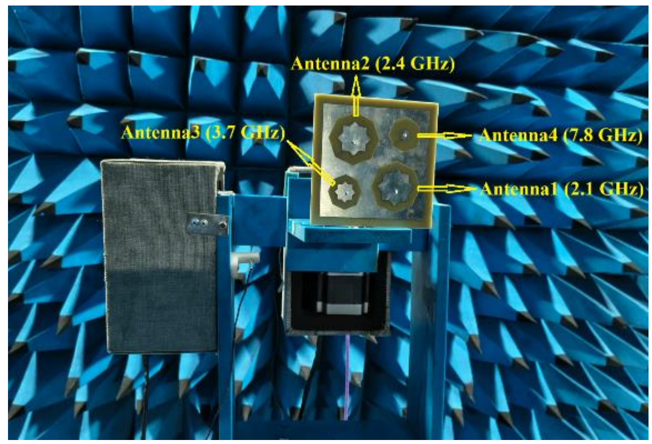

(b)

Fig. 4 Experimental setup (a) VNA connected, (b) Anechoic chamber.

4.1. Experimental Setup

A tuned Vector Network Analyzer (VNA) was employed to quantify the transmission coefficients (S_{xy}), reflection coefficient (S_{11}), and VSWR by individually probing each antenna under matched load conditions. The measurement setup, including VNA connection with probed fixture configuration, is depicted in Figure 4 (a), and gain measurement in an anechoic chamber is shown in Figure 4 (b).

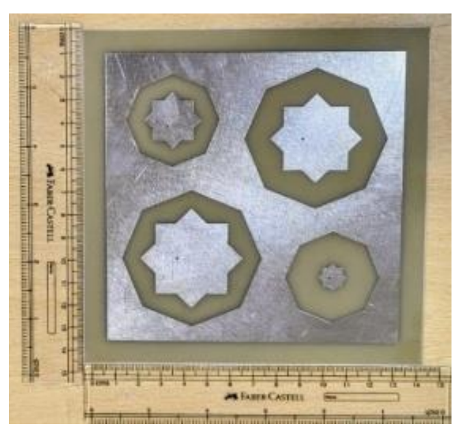

(a)

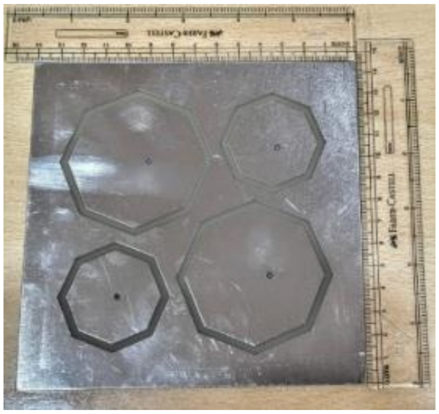

(b)

Fig. 5 Fabricated Prototype of shared-aperture antenna, (a) Upper layer, (b) lower layer view.

A fabricated prototype of the antenna is illustrated in Figure 5 with top and bottom views. The top view shows the etched radiating patch with four slot-loaded elements, while the bottom view shows the segmented ground structure that was used to eliminate inter-band coupling. For completeness, Figure 6 shows the back view with SMA connectors.

Fig. 6 Fabricated antenna back view showing SMA connectors integration and segmented ground

Figure 7 illustrates the simulated and measured reflection coefficients (S_{11}) for all four frequency bands. The simulated traces exhibit excellent impedance matching and minimal reflection across all four ports. When we move to the measurement phase, we observe some minor shifts in both resonant frequency and the reflection coefficient values compared to simulation results. These variations are likely the result of fabrication tolerance and small imperfections during the soldering process. In spite of these small mismatches, the response of the modeled antenna remains consistently strong and acceptable across all the targeted frequency bands. To further refine the design and cross-verify the results obtained in simulation and measurements, we developed and simulated an equivalent circuit model to specifically analyse the reflection coefficient (S_{11}) at all four operating frequency bands.

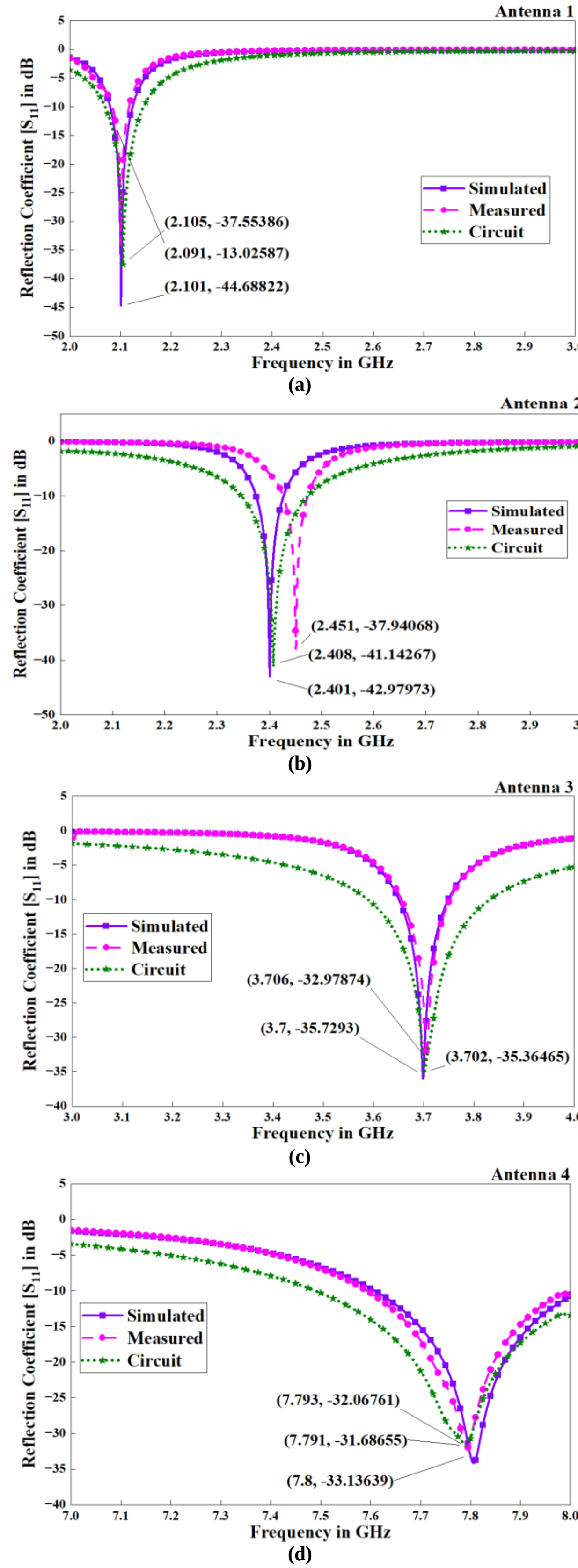

Fig. 7 Comparison of simulated, measured, and equivalent circuit S_{11} across all four bands.

The simulated VSWR values remain very near to unity, and these values represent excellent impedance matching and efficient power transmission from the feed system to each radiating patch element. Experimental findings further validate good behavior at their respective resonant points, as depicted in Figure 8. Since these metrics are in a reasonable range, the antenna is grounded for real-world use, as slight deviations arise from the manufacturing process.

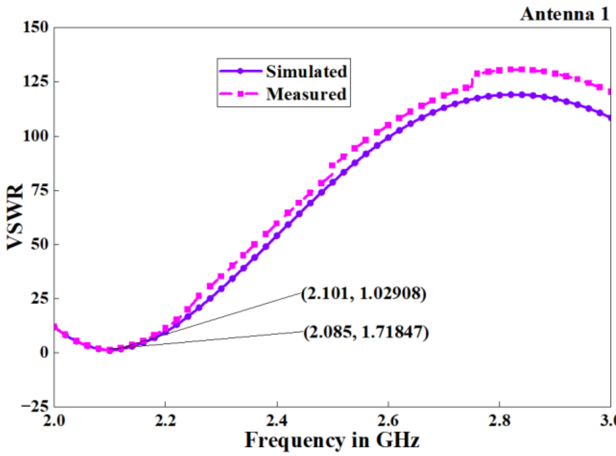

(a)

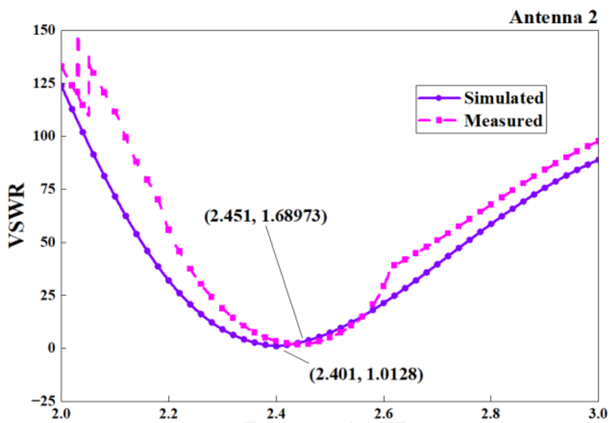

(b)

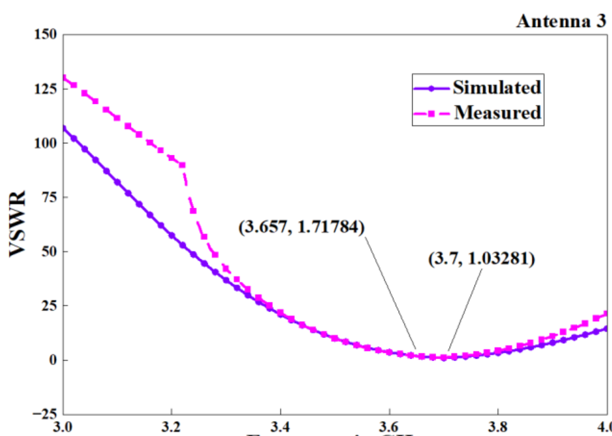

(c)

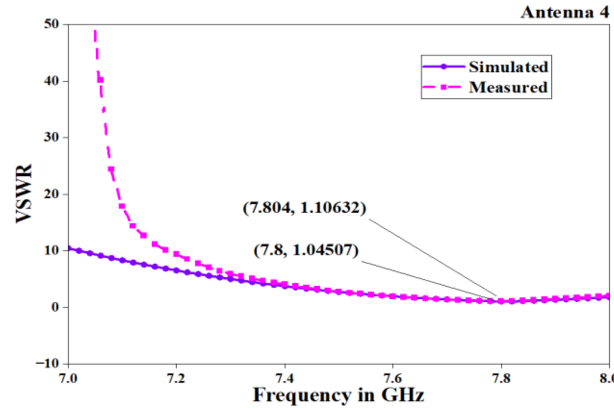

(d)

Fig. 8 Simulated and measured VSWR for all four frequency bands.

The simulated and measured isolation between all the port pairings of the quad-band antenna is depicted in Figure 9. The results exhibit strong isolation in both cases. The values ranging between $-30\,dB$ to $-67\,dB$ across the entire spectrum of interest. This is achieved by introducing a separate ground design and an optimized special arrangement of the shared substrate. This performance reveals that the mutual coupling between each port pairing is successfully suppressed. Reaching to this isolation level is mainly required for multiband systems, because they confirm reliable performance without any interference. The surface current distribution of the proposed antenna at 2.1 GHz, 2.4 GHz, 3.7 GHz, and 7.8 GHz is presented in Figure 10, further substantiates that the antenna achieves strong isolation with minimum overlap while maintaining efficient multiband operation.

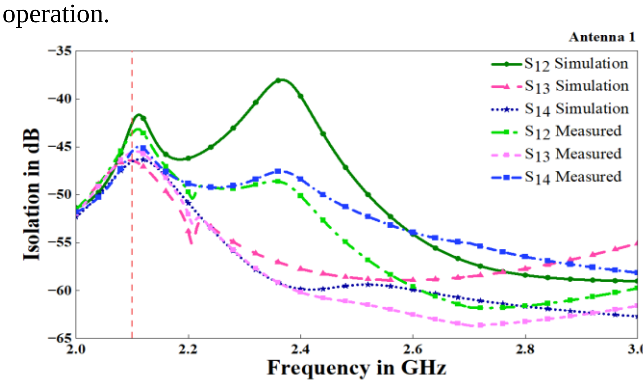

(a)

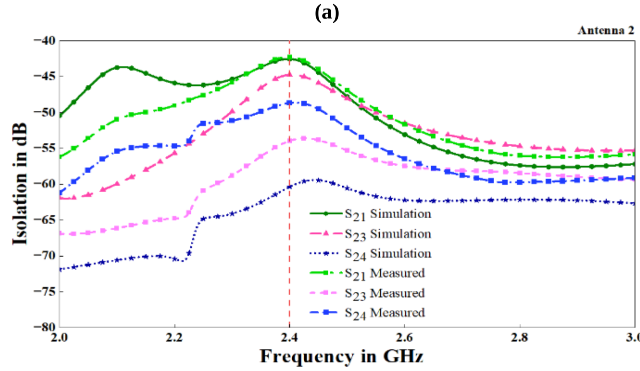

(b)

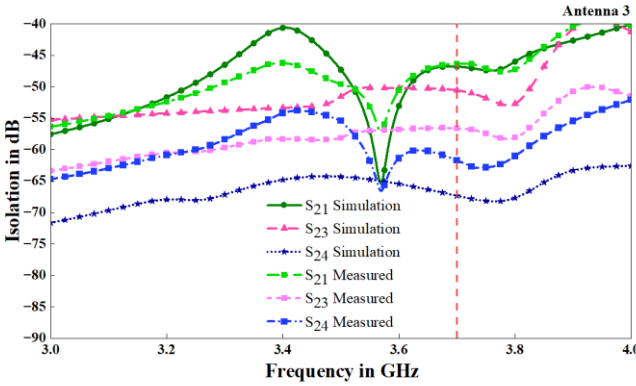

(c)

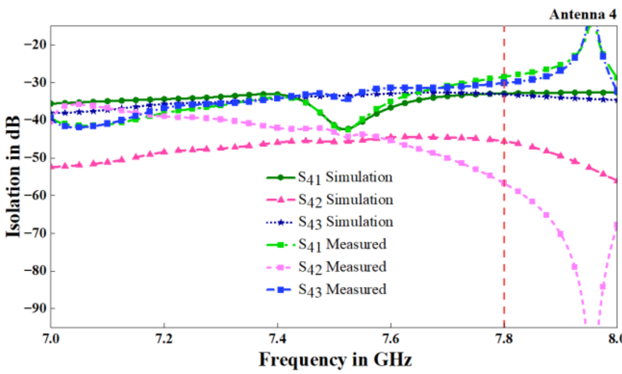

(d)

Fig. 9 Simulated isolation characteristics across all port combinations of the proposed antenna.

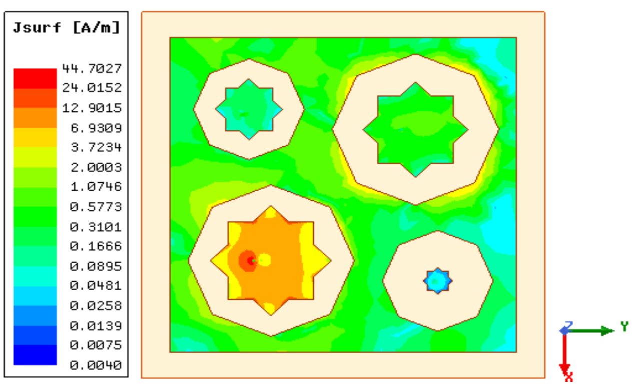

(a)

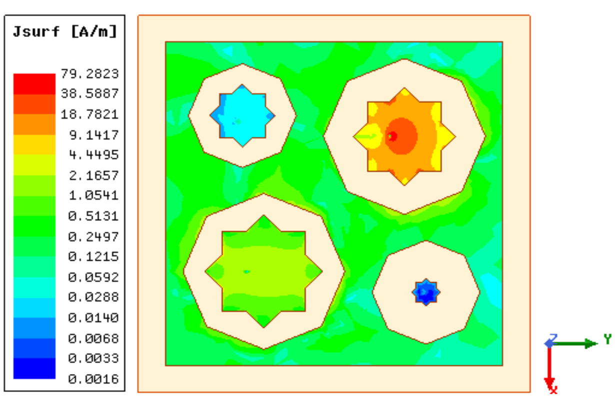

(b)

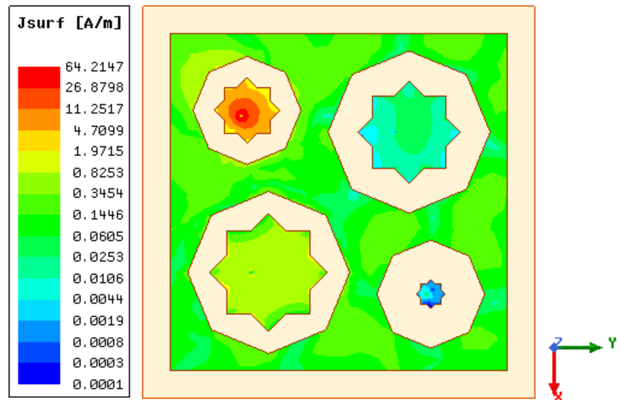

(c)

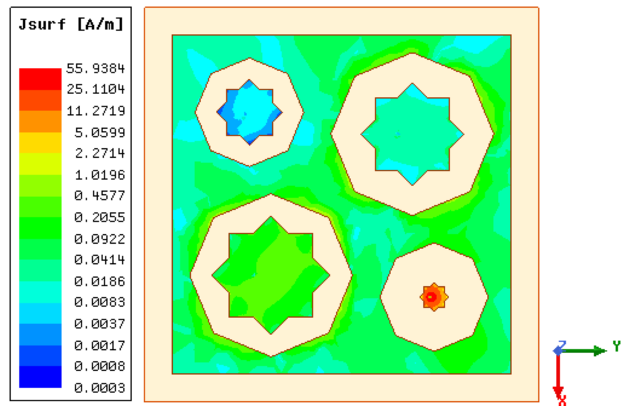

(d)

Fig. 10 **Surface current profile (simulation) at resonant frequency, (a) 2.1 GHz, (b) 2.4 GHz, (c) 3.7 GHz, (d) 7.8 GHz.**

Figure 11 presents the antenna gain variation with frequency, comparing modeled and observed results of the proposed antenna. The tested gain values follow the simulated gain values, confirming the precision of the design model. The measured gain traces lie in the range of 3.6 - 7.8 dBi. These values authenticating good agreement with the simulation across the operating bands. Minor deviations were observed in the upper frequency spectrum because of fabrication tolerances and measurement setup limitations, but overall, the consistency validates the antenna performance.

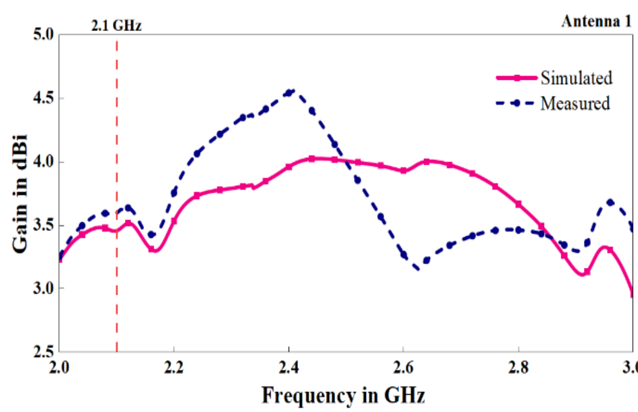

(a)

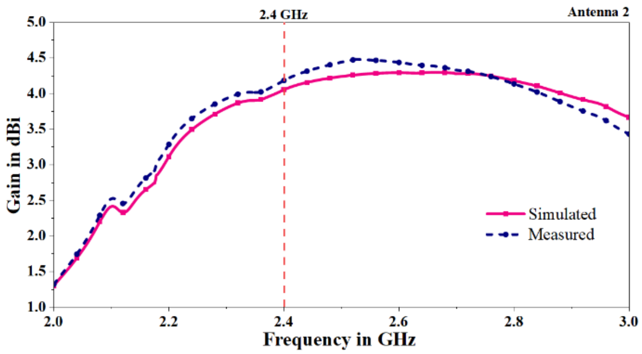

(b)

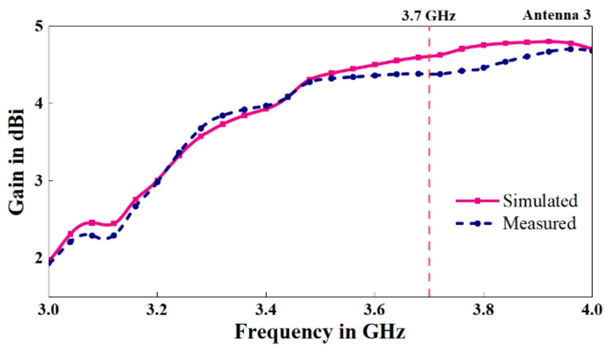

(c)

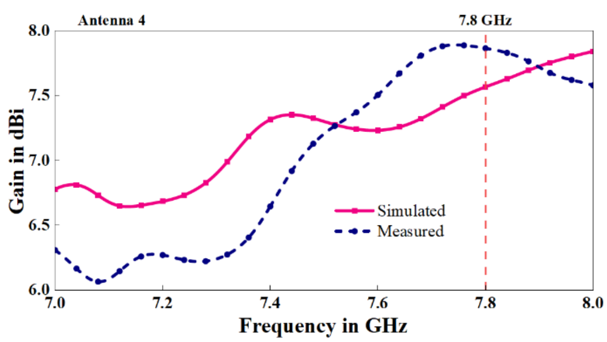

(d)

Fig. 11 Simulated and measured Gain plot at 2.1, 2.4, 3.7, and 7.8 GHz.

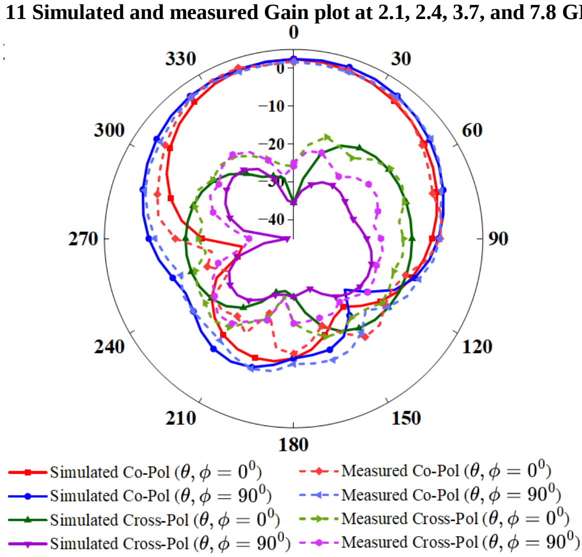

(a)

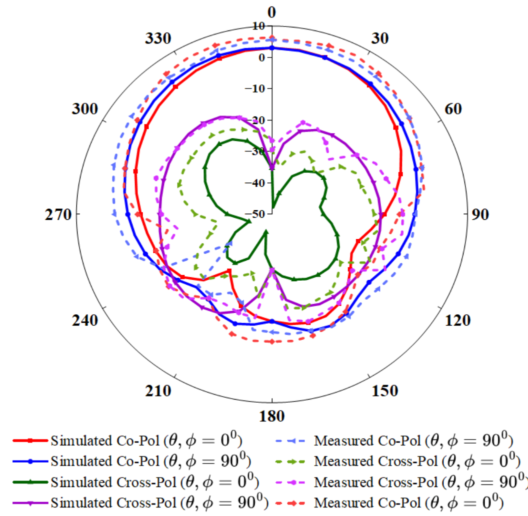

(b)

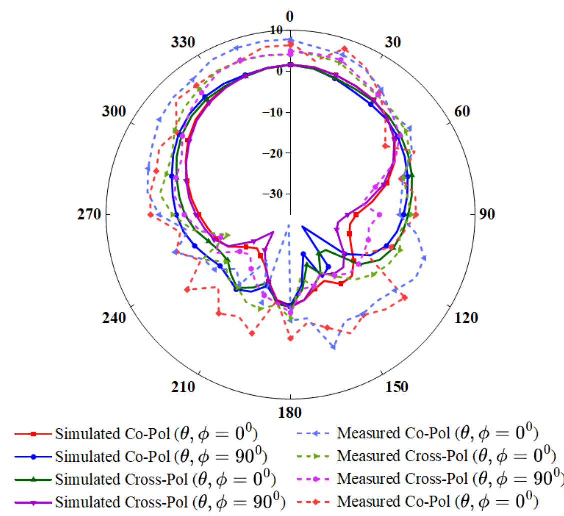

(c)

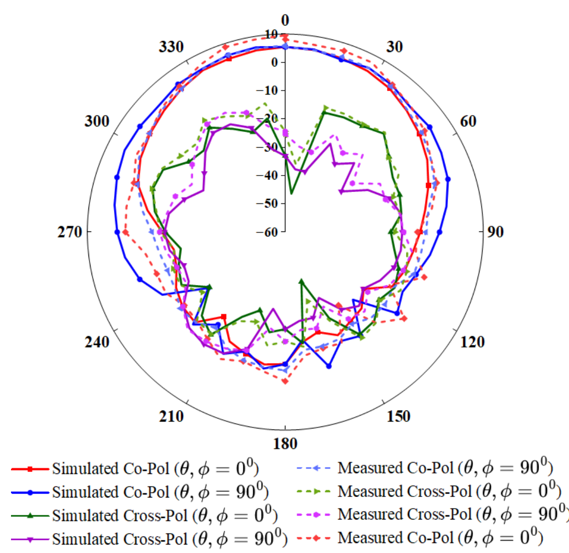

(d)

Fig. 12 Co-and Cross-Polar Radiation Patterns (H- and E-Planes) (simulated and measured) at 2.1, 2.4, 3.7, and 7.8 GHz.

The comparison of modeled and measured cross-polarization and co-polarization characteristics in both E- and H-planes across all four operating frequencies (2.1, 2.4, 3.7, and 7.8 GHz) is presented in Figure 12. The antenna performance in terms of directional radiation is illustrated by each plot, highlighting the agreement between simulation results and experimental validation. The co-polarization curves present the overall strength of the radiation and major lobe orientation.

The cross-polarization curves confirm polarization purity by indicating the level of unwanted polarization. Altogether, the results validate the design's accuracy and reliability across multiple bands.

The measured and simulated performance of the shared aperture antenna in quad-band operation is showcased in the Table 3. The comparison with the related reported literature is presented in the Table 4. The segmented ground structure and octa-star patch antennas with spatial separation result in no inter-band coupling. These results confirm that the multiband antenna will work consistently in a small aperture.

The four resonant frequency bands are achieved by scaling the octa-star geometry using Equation (3). While the frequency bands are quite small, their allocation align to standard frequencies: LTE (2.1 GHz), Wi-Fi / IoT (2.4 GHz), 5G sub-6 (3.7 GHz), and emerging mid-band (7.8 GHz). The symmetry of octa-star geometry is adapted to enable the individual elements to minimally couple.

With a footprint of $145\ mm \times 145\ mm \times 1.6\ mm$, the antenna can be suggested to integrate into IoT modules, CubeSat payloads, and 5G devices. The equivalent circuit results closely match full- wave simulations, with deviations less that 5%, confirming the validity of the lumped element model.

4.2. Key Contributions

The proposed work offers:

- Quad band operation (2.1, 2.4, 3.7, 7.8 GHz) within a shared aperture.
- Compact octa-star geometry enabling resonance separation.
- High isolation (>30 dB) via segmented ground design.
- Equivalent circuit validation against full-wave simulations.
- Suitability of CubeSat, IoT, and vehicular communication systems.

Table 3. Measured and simulated performance summary across all bands

Metric	2.1 GHz	2.4 GHz	3.7 GHz	7.8 GHz
Simulated S_{11} (dB)	-44.68	-42.97	-35.73	-33.14
Measured S_{11} (dB)	-39.39	-37.94	-29.91	-31.69
Circuit Simulated S_{11} (dB)	-37.55	-41.14	-39.02	-32.07
Simulated VSWR	1.02	1.03	1.04	1.02
Measured VSWR	1.72	1.69	1.71	1.10
Simulated Gain (dBi)	3.45	4.12	4.67	7.56
Measured Gain (dBi)	3.62	4.22	4.34	7.87
-10 dB Bandwidth (MHz)	40	60	100	340
Simulated Isolation (dB)	-42.51 to -46.52	-42.55 to -60.36	-46.78 to -67.34	-32.88 to -45.56
Measured Isolation (dB)	-43.47 to -46.12	-42.27 to -53.93	-46.35 to -61.49	-28.40 to -56.55

Table 4. Performance validation of the proposed antenna with the previously reported shared aperture antenna

Reference	Aperture Type	Frequency Bands	Dimension (mm)	Gain (dBi)	Max. Isolation (dB)
[5]	Insertion	L, X, K, Ka	100 × 100 × 0.79	3.06	-35
[6]	Insertion	S, X	60 × 60 × 20	7.07	-25
[7]	Stacked	C, X, Ku, K, Ka	100 × 100	6.5	-60
[11]	Stacked	L, S, C	200 × 200 × 1	5.3	-35
Proposed work	Insertion	S, C	145 × 145 × 1.6	7.8	-67

5. Conclusion

This research exhibits a novel quad-band shared aperture antenna that addresses the needs of wireless communication and 5G technology. The antenna emphasizes an innovative configuration in which octa-star-shaped patches are arranged within an octa-gram slot, with each patch optimized to operate within a specific frequency range.

In the proposed antenna, the radiating patches were carefully arranged in a uniform pattern, with each one supported by its own dedicated ground structure. This arrangement will significantly reduce interference among the desired four frequency bands. The resultant quad-band antenna is efficient, and it is capable of providing multiple frequencies within a single design. Therefore, the proposed antenna is suggested for devices that require compatibility with various communication applications, such as smartphones, IoT hubs, and 5G equipment.

In summary, this antenna design provides a versatile and optimized solution for embedding multiple frequency capabilities into wireless devices where space is a constraint.

References

[1] Ying Sun et al., "Tri-Band Dual-Polarized Shared-Aperture Antenna Arrays With Wide-Angle Scanning and Low Profile for 5G Base Stations," *IEEE Transactions on Antennas and Propagation*, vol. 72, no. 3, pp. 2455-2467, 2024. [CrossRef] [Google Scholar] [Publisher Link]

[2] Yihong Su et al., "Design Guidelines of Stacked Dual-Band SIW Slot Array with Optimal Aperture Reuse Ratio and High Aperture Efficiency," *IEEE Open Journal of Antennas and Propagation*, vol. 6, no. 3, pp. 797-809, 2025. [CrossRef] [Google Scholar] [Publisher Link]

[3] Donglin He, Yikai Chen, and Shiwen Yang, "A Multiband Dual-Polarized Shared-Aperture Antenna Array," *2021 IEEE International Symposium on Antennas and Propagation and USNC-URSI Radio Science Meeting (APS/URSI)*, Singapore, Singapore, pp. 1791-1792, 2021. [CrossRef] [Google Scholar] [Publisher Link]

[4] Jia Cheng et al., "Dual-Band Shared-Aperture Antenna with Pattern and Polarization Diversity," *Applied Sciences*, vol. 15, no. 2, pp. 1-14, 2025. [CrossRef] [Google Scholar] [Publisher Link]

[5] Md Nazim Uddin, and Elias A. Alwan, "A Shared-Aperture Pentaband Antenna with High Impedance Surface for CubeSat Application," *Scientific Reports*, vol. 14, no. 1, pp. 1-12, 2024. [CrossRef] [Google Scholar] [Publisher Link]

[6] Syed Salman Kabir, Mehedi Hassan Khan, and Saeed I. Latif, "A Multi-Band Circularly Polarized-Shared Aperture Antenna for Space Applications at S and X Bands," *Electronics*, vol. 12, no. 21, pp. 1-11, 2023. [CrossRef] [Google Scholar] [Publisher Link]

[7] Hesham M. Elkady, Haythem H. Abdullah, and Saad M. Darwish, "Multiband Circularly Polarised CubeSat Antenna Operating in S, C, X, Ku, K, and Ka Bands," *IET Microwaves, Antennas & Propagation*, vol. 18, no. 2, pp. 82-95, 2024. [CrossRef] [Google Scholar] [Publisher Link]

[8] Yuanming Xiao, Lianxing He, and Xiaoli Wei, "Dual-Band Dual-Circularly Polarized Shared-Aperture Phased Array for S-/C-Band Satellite Communications," *Electronics*, vol. 14, no. 2, pp. 1-13, 2025. [CrossRef] [Google Scholar] [Publisher Link]

[9] Changpeng Ji, Xin Ning, and Wei Dai, "Design of Shared-Aperture Base Station Antenna with a Conformal Radiation Pattern," *Electronics*, vol. 14, no. 2, pp. 1-20, 2025. [CrossRef] [Google Scholar] [Publisher Link]

[10] Harri Varheenmaa et al., "Wideband Shared-Aperture Antenna for Full-Screen 5G Mobile Devices," *IEEE Access*, vol. 12, pp. 151507-151514, 2024. [CrossRef] [Google Scholar] [Publisher Link]

[11] Chuang Wang et al., "A Low-Profile Tri-Band Shared-Aperture Antenna for Sub-6G Wide-Beam and Millimetre-Wave High-Gain Applications," *IET Microwaves, Antennas & Propagation*, vol. 18, no. 12, pp. 932-943, 2024. [CrossRef] [Google Scholar] [Publisher Link]

[12] Zhi Jing Xiao et al., "Dual-Band Shared-Aperture Base-Station Antenna Array With Dual Polarization Using Filtering Magnetoelectric Dipole Antenna," *IEEE Open Journal of Antennas and Propagation*, vol. 5, no. 1, pp. 82-89, 2024. [CrossRef] [Google Scholar] [Publisher Link]

[13] Md Abu Sufian et al., "A Shared Aperture Multiport Antenna for Rural Wireless Communication and Safety Monitoring using TVWS, ISM, and 5G mmWave Bands," *Scientific Reports*, vol. 15, no. 1, pp. 1-16, 2025. [CrossRef] [Google Scholar] [Publisher Link]

[14] Yuan Zhang et al., "Dual-band and High-Isolation Shared-Aperture Antenna for Broadband Airborne Applications," *Journal of Electronic Science and Technology*, vol. 22, no. 4, pp. 1-11, 2024. [CrossRef] [Google Scholar] [Publisher Link]

[15] Jiyoung Park et al., "Design of a Dual-Band Shared-Aperture Array Antenna Composed of Array Elements with High Electromagnetic Transparency," *IEEE Access*, vol. 12, pp. 137533-137541, 2024. [CrossRef] [Google Scholar] [Publisher Link]

[16] Mingtang Li et al., "A Versatile Shared-Aperture Antenna for Vehicle Communications," *Electronics*, vol. 13, no. 20, pp. 1-15, 2024. [CrossRef] [Google Scholar] [Publisher Link]

[17] Constantine A. Balanis, *Antenna Theory: Analysis and Design*, 4th ed., John Wiley & Sons, Hoboken, pp. 1-1104, 2016. [Google Scholar] [Publisher Link]